

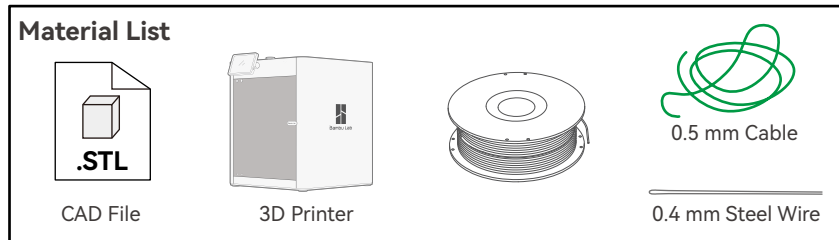
**DEVICE, Volume 3**

**Supplemental information**

**SpiRobs: Logarithmic spiral-shaped robots  
for versatile grasping across scales**

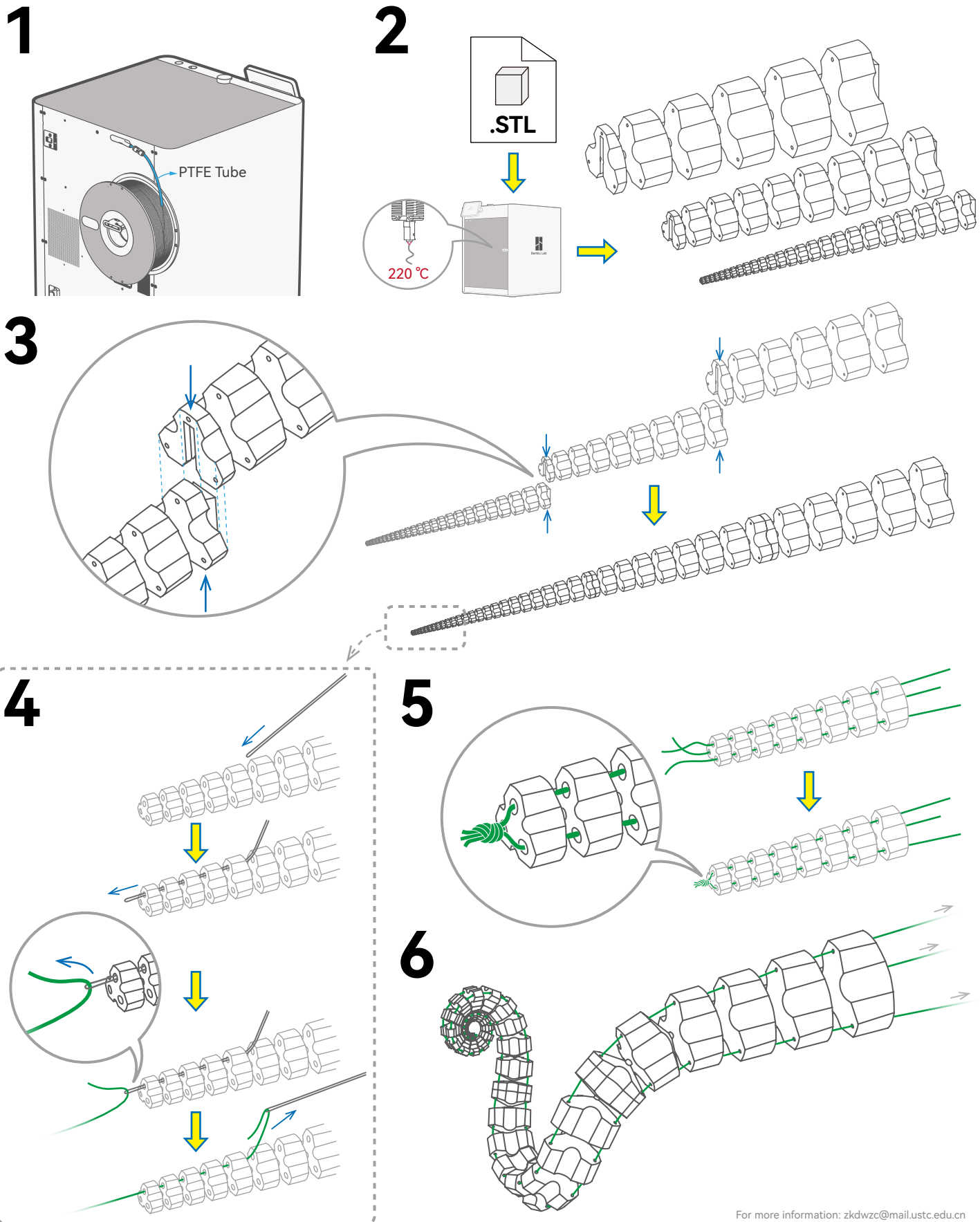
**Zhanchi Wang, Nikolaos M. Freris, and Xi Wei**

## Supplemental Experimental Procedures



# SpiRob

Fabrication Instructions



For more information: zkdwzc@mail.ustc.edu.cn

## Supplemental Notes

### Note S1. Fabrication of SpiRobs

The main body of the SpiRob is printed with Thermoplastic Polyurethane (TPU) using a Bambu Lab X1CC printer. Here are some important points to consider when printing:

- **Choose TPU with the appropriate hardness.** Different hardness levels of TPU will result in different robot stiffness. For example, there are options like 68D, 95A, and 83A (listed in descending order of hardness). We used eTPU 95A from eSUN Inc. because it ensures high printing quality (lower hardness levels have a higher risk of printing failure).
- **Keep TPU filament dry before use.** Dry the filament to prevent moisture-related issues like excessive stringing or oozing in the resulting prototype.
- **Feed TPU filament smoothly into the printer.** When using the 3D printer, do not use the Automated Material System (AMS). Instead, place the TPU directly on the rear spool holder or an external holder (see Supplemental Experimental Procedures for details). Ensure that the material spool turns smoothly to reduce resistance when feeding the material to the extruder.

We have included a .3mf file with the settings used for printing TPU. For more information on printing TPU filament, please refer to Bambu Lab's printing guide.

After printing, pass the cables through the robot (see Supplemental Experimental Procedures). You can use a 0.5 mm diameter UHMWPE (ultra-high molecular weight polyethylene) cable because it is soft, durable, and does not stretch easily. As the size of the units gets smaller towards the tip, the holes also become smaller, making it difficult to pass the cable through them. For this reason, use a stiffer, thinner steel wire to create a needle-like tool that helps guide the cable through the small holes (see Supplemental Experimental Procedures for a visualization). Afterwards, tie a knot at the tip of the robot and connect the other end of the cables to motors to drive the robot's movement.

In addition to the 3D printing method, we demonstrate a method for Origami fabrication of the robot using a sheet of paper (Figure S2D). The idea is to expand the body of the robot on a plane. Thanks to the proportional relationship between adjacent units, we can obtain the design of the entire robot from a two-dimensional expanded view of one unit. This method is similar to building Origami toys, in which the pattern printed on the paper needs to be cut out, bent, and glued in place. There is no specific design of an elastic layer, and the inner portion of the paper sheet serves this role. We demonstrate that the robot can grasp an apple (170 g, 34 times its self-weight) even when made with a sheet of paper (5 g). A 2-cable robot made in a similar way is shown in Figure S2E, comprising two 1-cable robots built separately and glued together. This Origami method is suitable for making 1- or 2- cable prototypes. It is difficult to fabricate 3-cable robots (capable of torsional deformations) this way.

### Note S2. Theoretical characterization of spiral robots

This section describes the theoretical analysis of the spiral robot's workspace, grasping range,

and load capacity. We take a 2-cable robot as an example for illustration. The workspace envelope can be obtained through the following process: each robot unit rotates from the one closest to the base, one joint at a time, while the other units are maintained as a straight line during the rotation process. Consequently, the envelope can be characterized by serially connected arcs drawn by the tip at each stage of the rotation process (Figures 2E and S4A). It is, therefore, approximately captured by the involute of the central spiral ( $\rho_c$ ), which is another logarithmic spiral ( $\rho_w$ , see Figure S4B):

$$\rho_w = \frac{a}{2b} (e^{2\pi b} + 1) e^{b(\theta - \frac{\pi}{2})}.$$

We can infer that the larger  $b$  is (i.e., larger taper angle  $\phi$ , as can be seen by taking the derivative in (3) to establish that  $\phi$  is increasing in  $b$ ), the faster the change of radius with angle, and thus the smaller the working space (obtained by varying  $\theta \in [0, \theta_0]$ ): this is in alliance with our simulation results (Figure 2E), which further attest that all points inside the envelope are reachable (the points in Figure 2E are obtained by inputting random control signals and recording the trajectory of the tip). This contrasts sharply with existing soft robots whose workspace is limited by the deformation rate, resulting in an almost spherical shell-like region<sup>[S1]</sup>.

To study the effect of the discretization, we consider the difference in swept area between the multi-unit robot based on discretization ( $S_1$ ) and a continuous spiral-shaped body ( $S_2$ ) (see Figure S4A and B):

$$S_1 = L(\theta) \Delta\theta, \quad S_2 = \int_{\theta-\Delta\theta}^{\theta} L(\theta) d\theta, \quad (10)$$

$$\eta = \frac{S_2}{S_1} = \frac{1}{b} \left( \frac{1-e^{-b\Delta\theta}}{\Delta\theta} \right). \quad (11)$$

In particular, note that  $\eta$  is independent of  $\theta$ . This establishes a uniformly bounded approximation error, which goes to 0 ( $\eta \rightarrow 1$ ) as  $\Delta\theta \rightarrow 0$ . This analysis was carried out for the 'virtual' tip (where two outer contours of the robot meet, i.e.,  $\theta \rightarrow -\infty$ ) solely for notational simplification.

After grasping the object, the workspace can also be analyzed using a similar geometric approach (Figure S4C). The idea is to regard grasping as a loss of a portion of the effective length. To calculate this loss, we consider the central axis of the portion used to grasp the object (the blue dashed line around the object in Figure S4D), which is a spiral characterized by:

$$\rho'_c(\theta, d) = \frac{d+\delta(0)}{2} e^{\cot \frac{\pi-\phi}{2} \theta}, \quad (12)$$

where the tangential angle is  $\frac{\pi-\phi}{2}$  and  $\delta(0)$  is the width of the tip. The length required to grasp an object with a diameter of  $d$  (assuming the object is circular and the robot wraps a fraction  $n$  of the circumference;  $n \geq 50\%$  is taken as the lower bound for wrapping to grasp the object) is given by:

$$L_{\text{grasp}} = \int_0^{2\pi n} \sqrt{{\rho'_c}^2 + {\dot{\rho}'_c}^2} d\theta. \quad (13)$$

The remaining length is  $L' = L - L_{\text{grasp}}$ . By fixing  $L'$  and repeating the analysis procedure, we

obtain the workspace envelope after grasping the object: it approximately follows another logarithmic spiral.

As for the size that can be grasped, the theoretical minimum diameter is  $d_{\min} = \rho(0) + \rho(\pi) = a + ae^{b\pi}$ , which corresponds to the diameter of the inscribed circle when the robot is packed into a spiral. For fixed width of the tip  $\delta(0)$ , a constraint is introduced between  $a$  and  $b$  as

$$a = \frac{\delta(0)}{e^{2\pi b} - 1}, \text{ which further implies:}$$

$$d_{\min} = \frac{\delta(0)(e^{\pi b} + 1)}{e^{2\pi b} - 1}. \quad (14)$$

The maximum diameter that can theoretically be grasped satisfies the following equation (Table S1):

$$L = \int_0^\pi \sqrt{\rho'_c(\theta, d_{\max})^2 + \dot{\rho}'_c(\theta, d_{\max})^2} d\theta. \quad (15)$$

This can be translated as the full length of the robot used to wrap 1/2 of the object's circumference (deemed as the bare minimum for grasping by wrapping). From (14) and (15), it can be inferred that the larger  $b$  is (which corresponds to a larger taper angle; see (3)), the smaller the maximum/minimum diameter of an object that the robot can grasp.

In reference to the load that can be grasped, we consider the situation shown in Figure S4C, where the cable force has reached its maximum value. In this case, increasing the object's diameter or its mass (or both) will cause the grasp to fail. This can be analyzed by means of torque balance:

$$M_{\max} g \rho'_c(\pi, d) = F_{\max} \left( \rho'_c(\pi, d) - \frac{d}{2} \right), \quad (16)$$

where the left side is the gravitational torque that aims to unfold the robot, and the right is the actuation torque. Based on (12), (14), and (15), we can derive the relationship between the taper angle and the mass/diameter of the grasped object (the expression is shown in Table S1, and the results are plotted in Figure 2F). Note that, to simplify the analysis, we ignore the elastic force exerted from the elastic layer, the friction between the cable and the body, and the deformation of the units: the extreme case analyzed here is thus a theoretical upper bound on the load value.

### Note S3. Modeling and simulation

To analyze the kinematic and dynamic behavior, we adopt the mechanism of a serial elastic joint (i.e., a series of links connected by joints) to simulate the spiral robot in MuJoCo (Figure S5A). For 2-cable robots, which can only bend on a plane, the adjacent units are connected with 1-DOF (degree of freedom) revolute joints. For 3-cable robots capable of deforming in the 3D space, we use 3-DOF ball joints to connect adjacent units (Figure S5B). The simulation of the cable-actuation mechanism uses the tendon-muscle class provided by MuJoCo. The viscoelasticity of the joints in the simulation is estimated directly from the material and geometric properties of the real robot (for example, the joint stiffness can be calculated from Young's modulus and the geometry of the elastic layer connecting the units). Note that since the adjacent units are proportional in scale, we only need to determine the parameters of one

link/joint (size, mass, viscosity, and elasticity), and the rest are derived by proportionality. For example, the ratio of mass is the third power of the ratio of unit length (assuming uniform density). It is critical to introduce limits for the robot joints in the simulation: correspond to a unit touching the next unit, i.e., are equal to  $\pm\Delta\theta$ . In particular, when all joints reach their upper/lower bound limits simultaneously, the robot is tightly packed into a logarithmic spiral.

#### Note S4. Evaluation of the bioinspired grasping strategy

Recall that our strategy is inspired by the octopus and consists of the following stages: extending the curled arms toward the object (*Reaching*), making contact with the object, and uncurling the arms along the surface to wrap around (*Wrapping*, Figure 3A, Video S3). We reproduce this strategy by controlling the cable forces. To verify its effectiveness, we conducted comparative experiments when this strategy was on or off (see Figure S6). When off, as the cable force increases, the robot starts to curl from the tip so that only objects within a limited range (close to the tip) can be successfully grasped. Objects at a larger (but still reachable) range will be missed (Figure S6A). In contrast, using the proposed bioinspired strategy, the robot can spread its tightly packed body in different directions and successfully wrap to grasp objects (Figure S6B). In addition, we quantitatively studied the grasping space of different-sized objects (Figure 3C). It is worth noting, in passing, that the sucker of the octopus also plays a very important role in grasping (complementary to wrapping); here, we only focus on reproducing the wrapping behavior and defer exploring the addition of suction cups to future work.

#### Note S5. Manipulating various objects

We use a 2-cable SpiRob (45cm in length) to demonstrate the ability to grasp and manipulate various objects. We tested for numerous objects varying in size, shape, and weight. We show that the same robot with the same strategy can successfully grasp and manipulate various objects (see Figure S7 and Video S6). Since visual perception and control were not the focus of these experiments, we manually controlled the two cables like a puppet.

We also tested the robot's ability to manipulate in confined spaces. The robot was used to move a pingpong to a designated position (Figure S8). The "Wrapping" behavior exhibited by the robot allows it to move on surfaces of varying roughness, turn around, and traverse a slit (Figure S8, Video S7).

#### Note S6. Remote control for the drone application

We built a control terminal for human teleoperation (Figures 5 and S2), which consists of three motors (M2006, DJI) and an embedded controller (Robomatser Development Board, type C, DJI). The terminal communicates with a joystick through a 2.4 GHz wireless channel and converts the commands into reference torque signals fed to the motors.

## Supplemental Tables:

**Table S1. Parameters for the design of a two-cable SpiRob**

Parameter	Symbol	Parameterized expression
Polar coordinate	$\theta$	-
Scaling factor	$a$	-
Scaling factor	$b$	-
Discretization step	$\Delta\theta$	-
Logarithmic spiral	$\rho(\theta)$	$ae^{b\theta}$
Central spiral	$\rho_c(\theta)$	$\frac{a}{2}(e^{2\pi b} + 1)e^{b\theta}$
Length of the central spiral from angle $\theta_1$ to $\theta_2$	$L(\theta_1, \theta_2)$	$\int_{\theta_1}^{\theta_2} \sqrt{\rho_c^2 + \dot{\rho}_c^2} d\theta = \frac{\sqrt{b^2 + 1}}{b} (\rho_c(\theta_2) - \rho_c(\theta_1))$
Length of the robot	$L(0, \theta_0)$	$L(0, \theta_0) = \frac{a\sqrt{b^2 + 1}}{2b} (e^{2\pi b} + 1) (e^{b\theta_0} - 1)$
Curvature at angle $\theta$ when packed into a spiral	$\kappa(\theta)$	$\frac{1}{\rho_c \sqrt{b^2 + 1}}$
Radius of curvature at $s$ ( $s \equiv L(-\infty, \theta)$ )	$r(s)$	$bs$
Taper angle of the robot	$\phi$	$2 \arctan\left(\frac{b(e^{2\pi b} - 1)}{\sqrt{b^2 + 1}(e^{2\pi b} + 1)}\right)$
Width of the robot at angle $\theta$	$\delta(\theta)$	$ae^{b(\theta+2\pi)} - ae^{b\theta}$
Ratio between adjacent units	$\beta$	$e^{b\Delta\theta}$
Involute of the central spiral (workspace)	$\rho_w$	$\rho_w = \frac{a}{2b} (e^{2\pi b} + 1) e^{b(\theta - \frac{\pi}{2})}$
Minimum diameter of an object that can be grasped	$d_{\min}$	$a(1 + e^{b\pi})$
Maximum diameter of an object that can be grasped	$d_{\max}$	$L = \int_0^\pi \sqrt{\rho'_c(\theta, d_{\max})^2 + \rho''_c(\theta, d_{\max})^2} d\theta$
Maximum load that the robot can hold (with diameter $d$ )	$M(\phi, d, F_{\max})$	$\frac{F_{\max}}{g} \left( 1 - \frac{d}{(d + \delta(0)) e^{\cot(\frac{\pi - \phi}{2}) \pi}} \right)$

**Table S2. Success rate of multi-SpiRob grasping (5 tests for each case)**



Objects	2-SpiRob array	4-SpiRob array	6-SpiRob array	8-SpiRob array
①	2/5	5/5	3/5	5/5
②	3/5	5/5	5/5	5/5
③	3/5	3/5	5/5	5/5
④	5/5	5/5	5/5	5/5
⑤	5/5	5/5	5/5	5/5
⑥	1/5	0/5	5/5	1/5
⑦	2/5	4/5	5/5	5/5
⑧	1/5	1/5	3/5	5/5
⑨	4/5	5/5	5/5	5/5
⑩	2/5	3/5	5/5	5/5
Average±SD	0.48±0.23	0.72±0.37	0.92±0.17	0.94±0.19

## Supplemental figures:

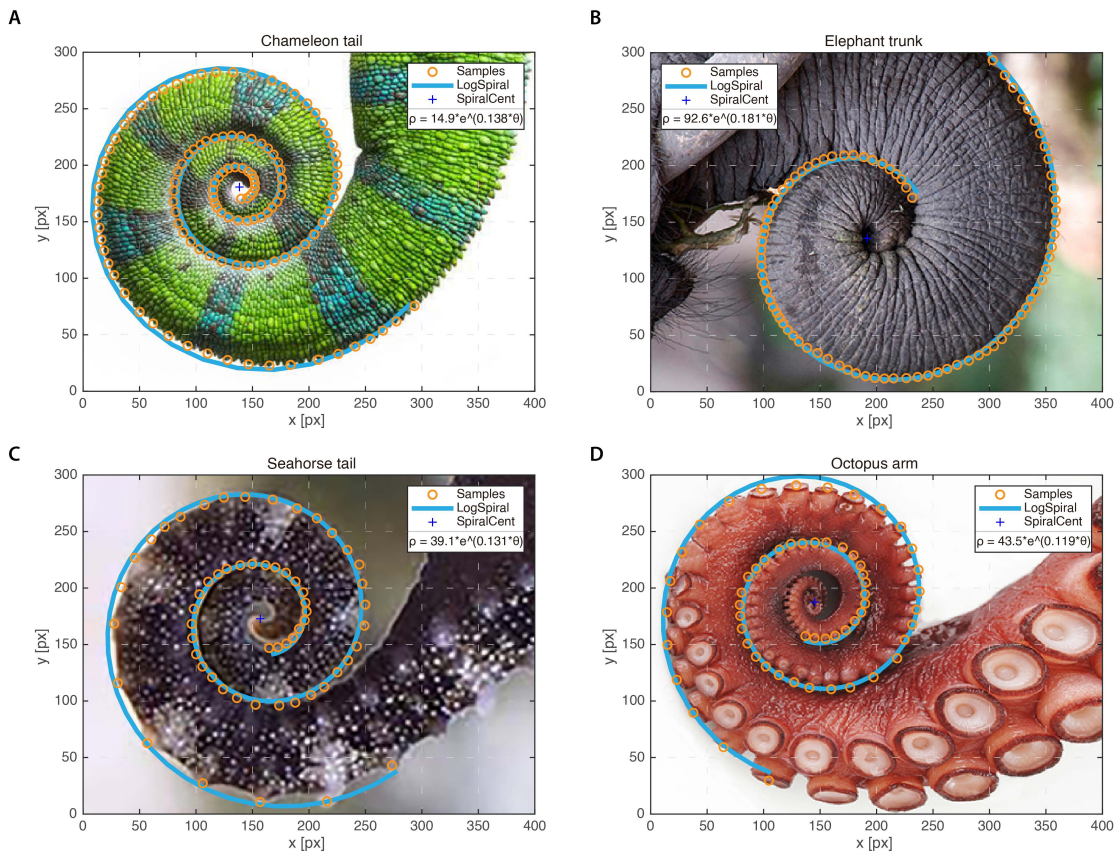


**Figure S1. Logarithmic spirals in nature. (A)-(D)** Fitting a logarithmic spiral to the chameleon tail, elephant trunk, seahorse tail, and octopus arm. The fitted parameters are shown for each case. We first cropped the image to 400x300 pixels and extracted points along the edges, then applied least squares fitting. All the pictures are from the Internet and were chosen so that the camera is perpendicular to the object to reduce the error caused by perspective.

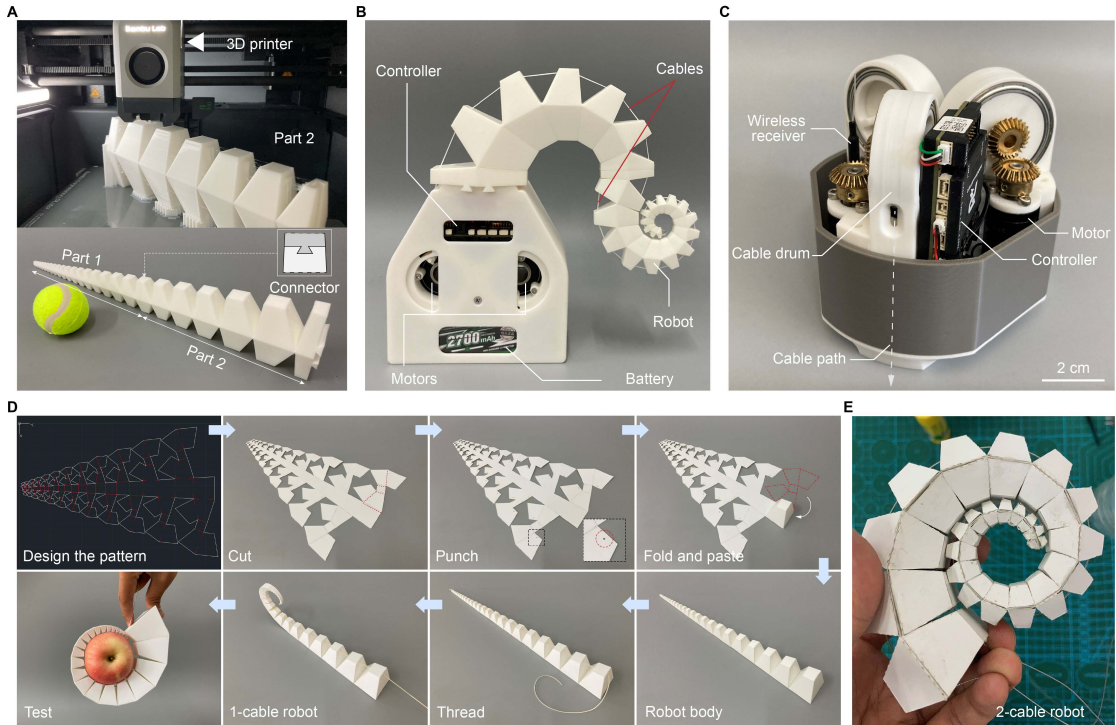


**Figure S2. Fabrication and assembly of robot components.** **(A)** Fabrication of robot body by 3D printing (first panel). Robots with different lengths can be obtained by printing parts separately and assembling them using connectors (dovetail shown in the second panel). **(B)** Hardware for driving a 2-cable SpiRob. The cables pass through the holes designed in each unit and are connected to DC motors. **(C)** The control terminal for 3-cable SpiRobs consists of three motors and an embedded controller. **(D)** Origami fabrication of SpiRobs. We first expanded the 3D model on a 2D plane, and then the robot was obtained by cutting, folding, and pasting a sheet of paper. We punch holes in the corresponding positions for the cable to pass. The spiral robots fabricated by this method are extremely light and can obtain a high load-to-weight ratio, but the maximum weight that can be grasped is, of course, smaller than robots made by 3D printing. **(E)** Picture of a 2-cable Origami SpiRob. Two 1-cable robots are glued back-to-back. The paper connecting the units constitutes the elastic layer.

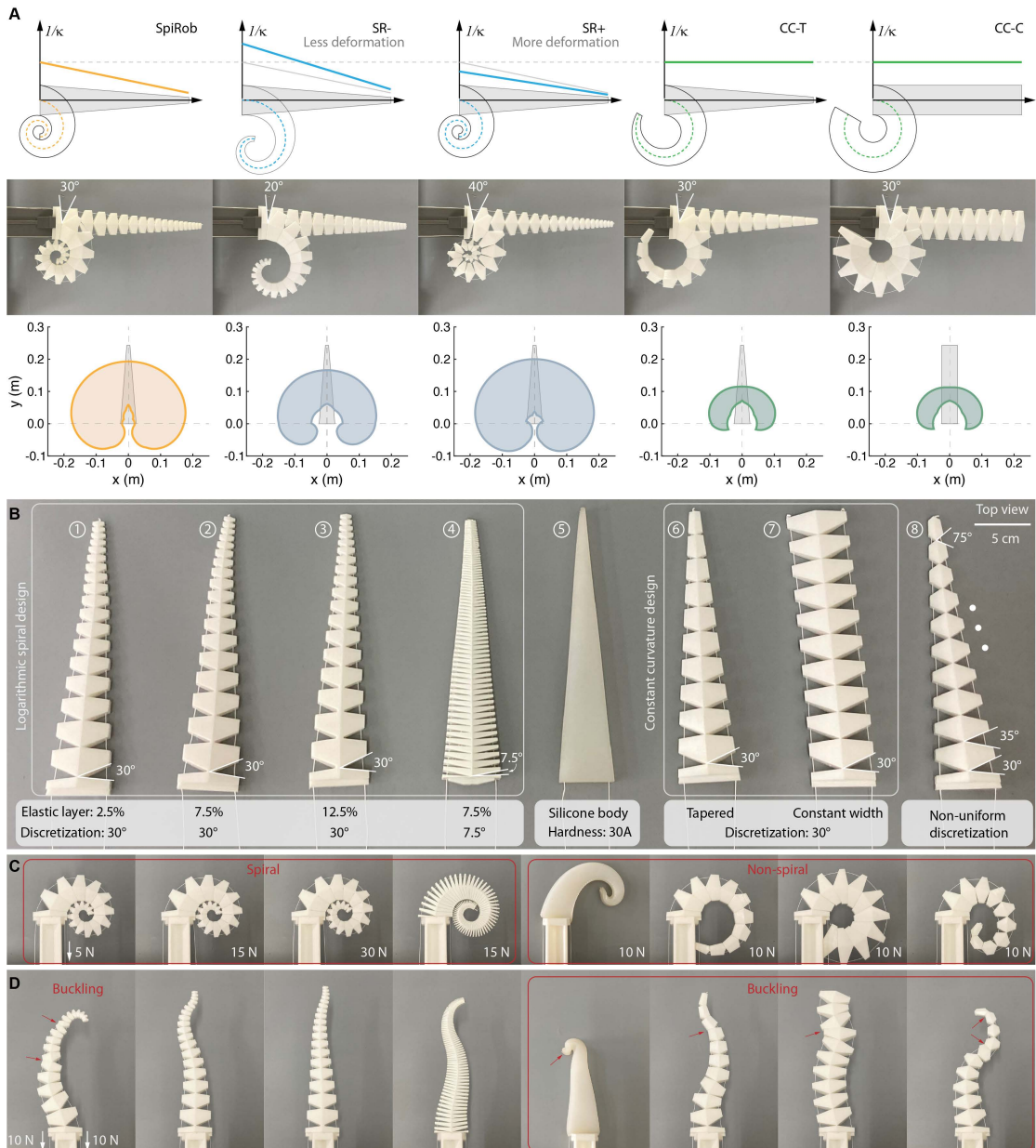


**Figure S3. Comparison of different designs. (A)** Prototypes for comparative experiments. SR- and SR+ are variants of our design with decreased/increased deformation ability (obtained by decreasing/ increasing the gaps by  $10^\circ$  while maintaining nominal lengths for each unit). CC-T is a tapered constant curvature robot<sup>[S2]</sup>, and CC-C is a cylindrical constant curvature robot. The workspaces for each of the different designs when holding the smallest graspable object are also plotted. **(B)** Prototypes of different SpiRobs (①-④) and non-spiral designs (⑤-⑧). **(C)** The cable is pulled on the right, and the actuation forces are marked in the lower right corner. For SpiRobs, the reported force is the minimum to attain tight packing. For non-spiral designs, the force is set as 10 N, and it is apparent from the visualization that they fail to achieve tight packing. **(D)** Applying antagonistic forces on the cables (10 N). For SpiRobs, thinner layers are easier to buckle (①). Smaller discretization steps can relieve buckling (④), but the fabrication is more challenging because units closer to the tip are getting smaller. Non-spiral designs tend to exhibit severe buckling under antagonistic forces.

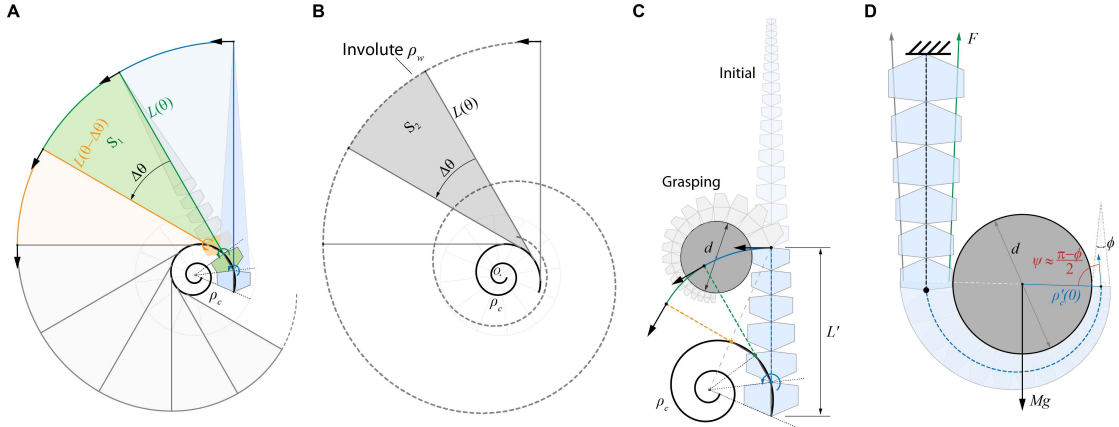


**Figure S4. Workspace and load analysis.** **(A)** Starting from the base, we progressively turn the joint of each unit until it touches the next unit. The tip draws arcs (illustrated as blue, green, and orange); this gives a piecewise arc approximation of the involute spiral. **(B)** The involute spiral ( $\rho_w$ ) approximately captures the envelope of the workspace. **(C)** With a similar approach, we can analyze the envelope when grasping an object. In this case, the point of interest is no longer the robot's tip but a point on the robot's body.  $L'$  is the length of the robot after grasping. **(D)** Load capacity analysis. We consider an object of fixed diameter  $d$  for increasing weight until the robot cannot wrap around more than 1/2 of its circumference (deemed a grasping failure). In this critical state, a torque balance between the actuation force ( $F$ ) and the weight of the object ( $Mg$ ) is achieved. This determines a theoretical upper bound on the maximum load capacity.

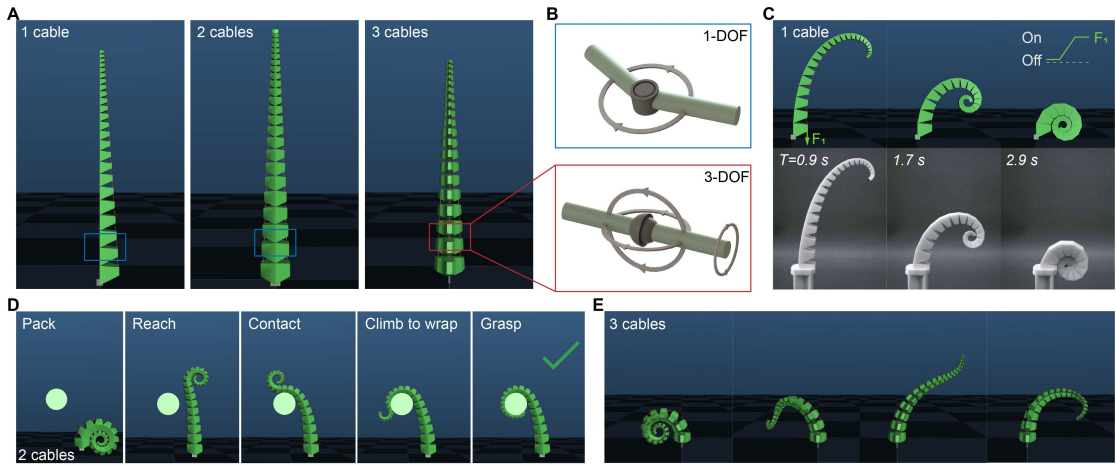


**Figure S5. Simulation of spiral robots.** **(A)** Images of 1-cable, 2-cable, and 3-cable SpiRobs in simulation. The first two are modeled using a series of 1-DOF revolute joints that connect the units, while the last uses 3-DOF ball joints (as shown in **(B)**). The rotational limits of the joints are set equal to the step size of the discretization (this corresponds to two adjacent units touching each other). The robot is completely packed into a logarithmic spiral when all joints have reached their limits. **(C)** Simulation (first panel) and demonstration (second panel) of the curling of the 1-cable robot. In this scenario, the actuation force of one cable ( $F_1$ ) is gradually increased until packing is attained. **(D)** Image sequences show the effectiveness of the grasping strategy in simulation. **(E)** Image sequences showing the 3D deformation of a 3-cable SpiRob in various configurations.

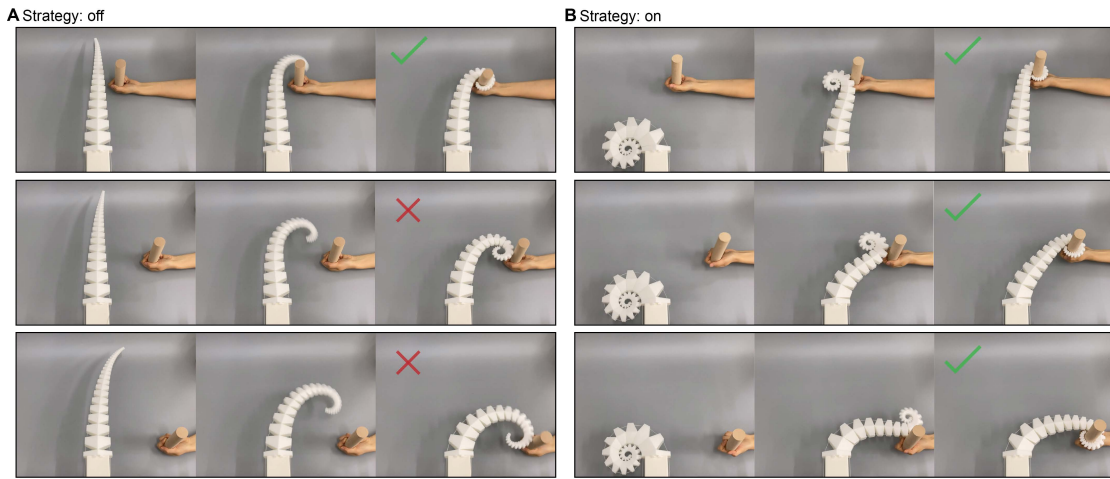


**Figure S6. Bioinspired grasping strategy. (A) (B)** Experiments to verify its effectiveness (Strategy: on) and comparison with a direct grasping attempt (Strategy: off). When the strategy is not used, the robot's grasping range is substantially limited ((A), second and third attempts fail). With the bioinspired strategy (B), the robot can reach out in different directions and climb along the surface of the objects to wrap and grasp them.

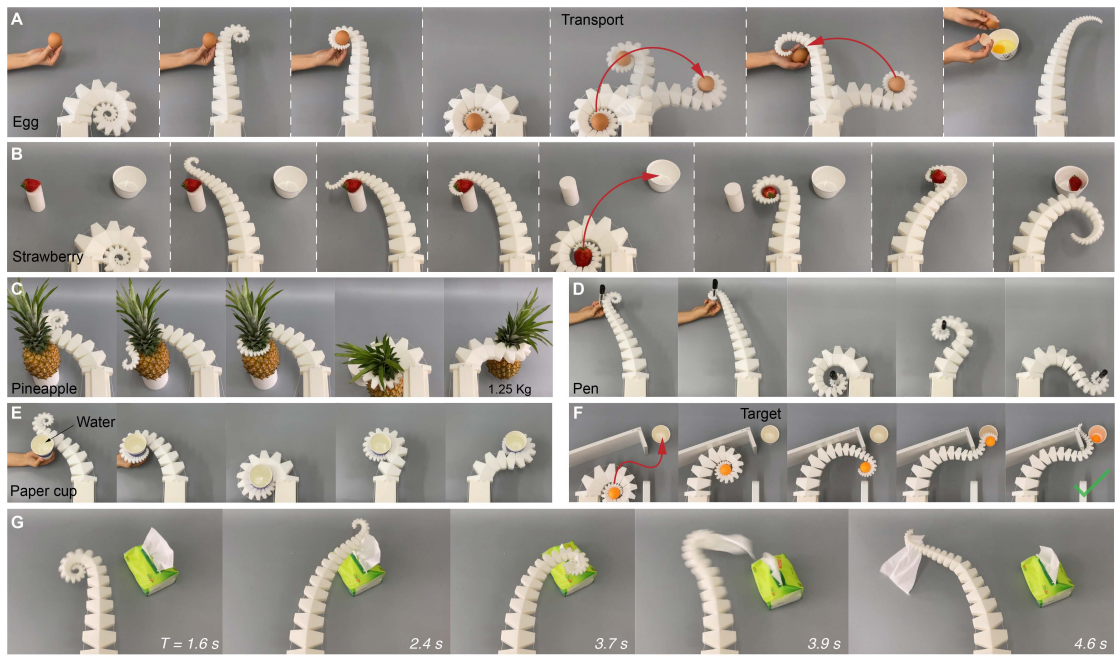


**Figure S7. SpiRobs grasping and transporting various objects.** (A)-(E) Image sequences of a 2-cable SpiRob handing a raw egg, a strawberry, a pineapple, a pen, and a paper cup filled with water. (F) The robot navigates through a door to transport a pingpong ball to its target in an S-shape trajectory. (G) SpiRob extracts tissue from a box resting on a table.

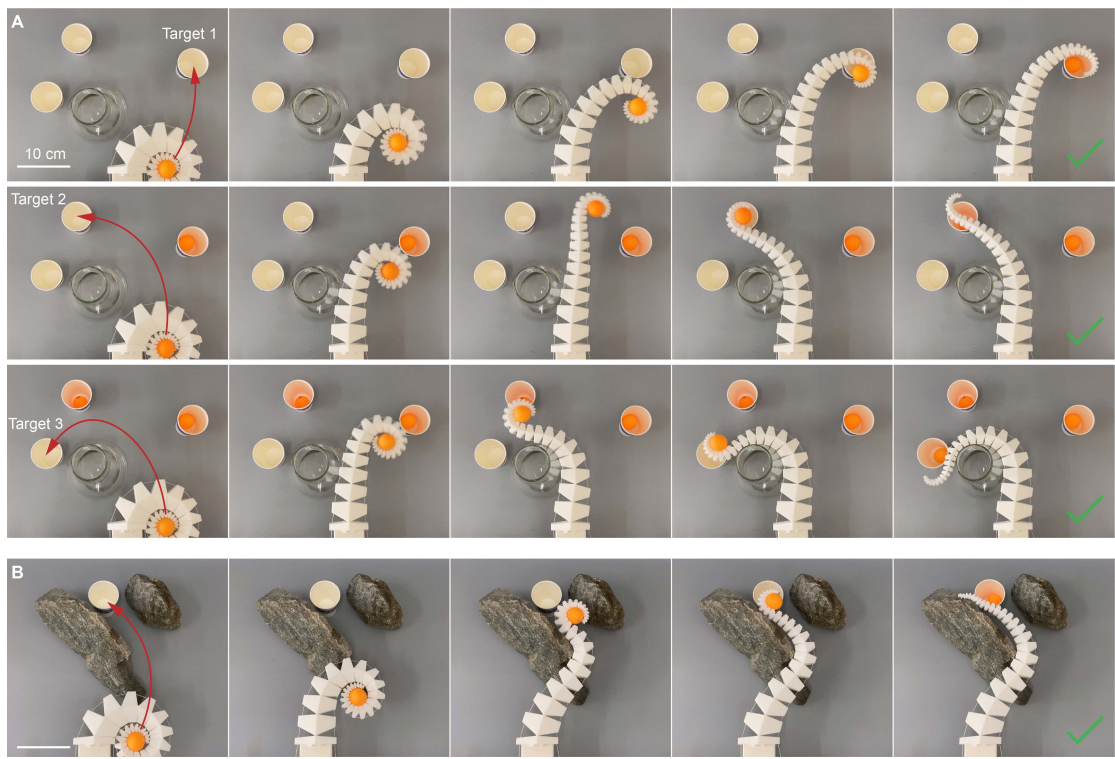


**Figure S8. Manipulation in confined spaces.** **(A)** Image sequences of the robot moving around a glass bottle to transport a pingpong ball to different targets. **(B)** The robot climbs on a rough stone surface and navigates through the two stones to drop the ball into the cup. These experiments were done by manually operating the two cables.

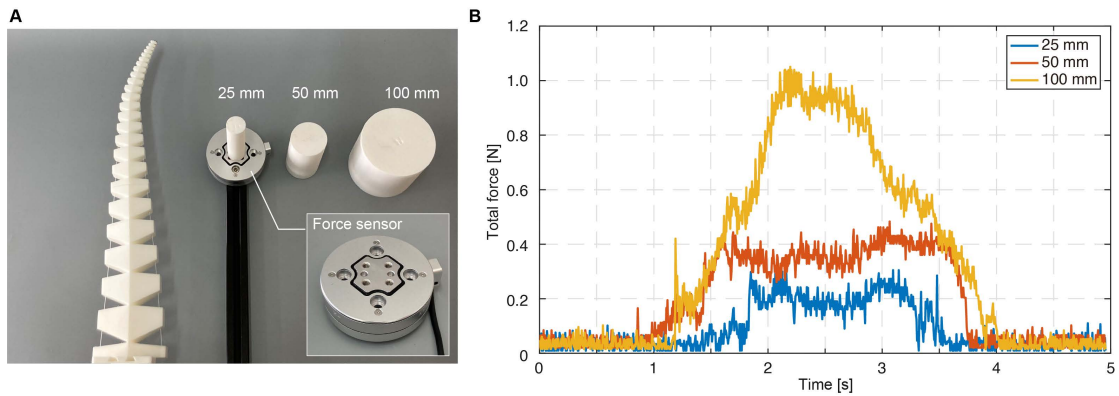


**Figure S9. Contact force.** **(A)** Experimental setup for measuring contact forces when the robot is climbing on the surface of an object. Objects of different diameters are placed on a force sensor (M4313A, SRI Inc.). **(B)** Measured force across time. The experimental results confirm that the wrapping process exerts force on the object, but the value remains low (and smaller for small objects).

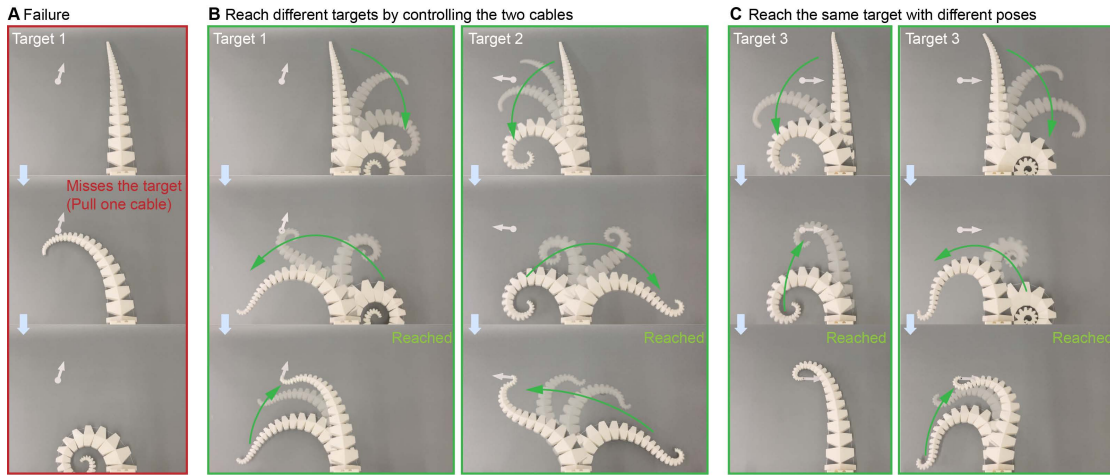


**Figure S10. Controllability of the tip.** **(A)** When only one cable is pulled, the whole robot's body curls and it is almost impossible to control the tip accurately to reach a target (target position and orientation are depicted with a solid white point and arrow). **(B)** By controlling two cables at the same time, different targets can be reached. The same goal can be reached with multiple poses **(C)**.

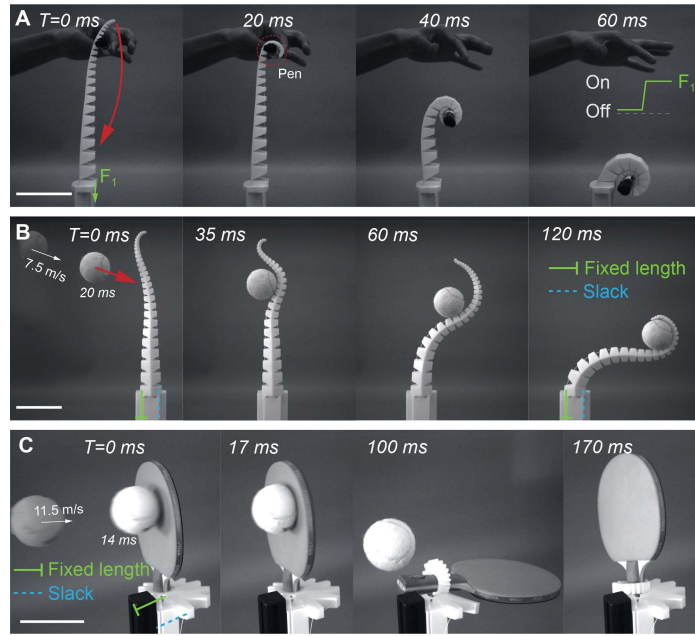


**Figure S11. Dynamic grasping.** **(A)** The robot grasps a pen and moves it to its base within 0.06s. The actuation pattern is displayed in the upper right corner where 'On' means the cable is stretched and 'Off' means the cable is slack. **(B)** Passive grasping. The robot can grasp a high-speed moving object within 120 ms without any control (the left cable is fixed to maintain a constant length while the right cable is slack). **(C)** The robot achieves a firm grasp of a pingpong racket, as demonstrated by throwing a tennis ball at high speed. Scale bars in (A)-(C) represent 10 cm.

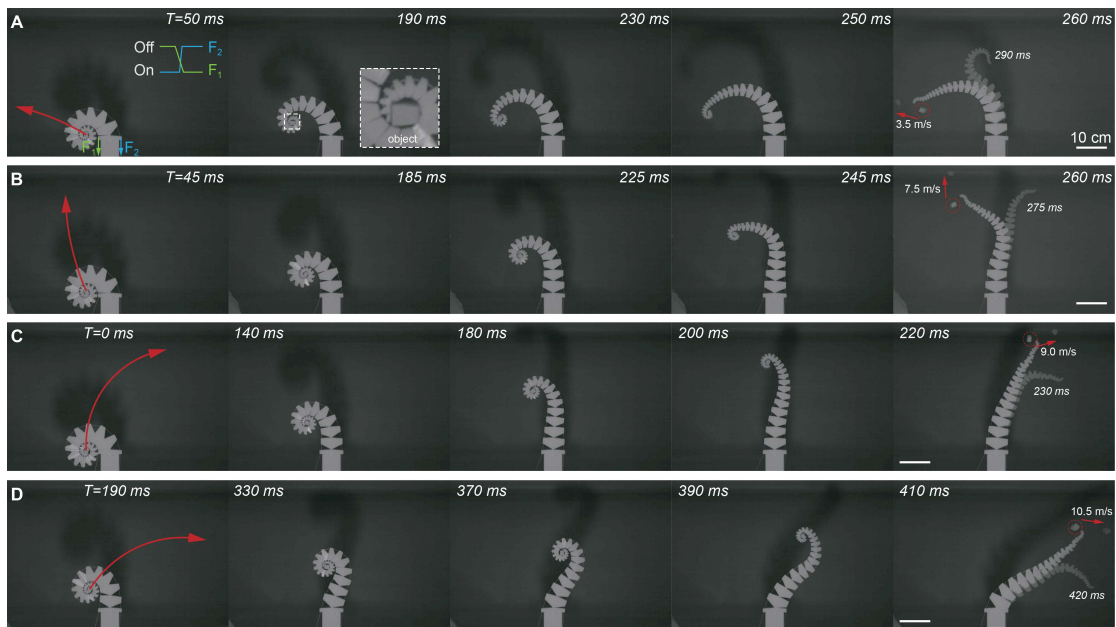


**Figure S12. Elephant throw. (A)-(D)** Image sequences of the robot throwing a piece of rubber in different directions. The robot starts from an initial state of wrapping the object and throws it out via an uncurling motion. Because of the rotation generated during the movement, the object flies out with a spin. From top to bottom, we observe that the longer the distance the robot moves with the object, the higher the velocity the object can obtain, with the highest release speed exceeding  $10\text{ m/s}$  (D). Controlling the rate of increasing/decreasing the two cables' forces makes it possible to generate different release directions.

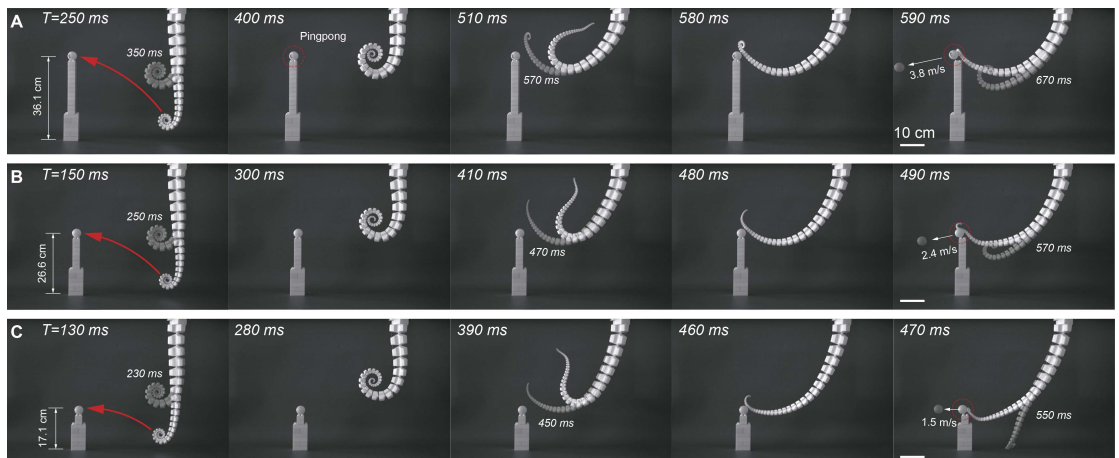


**Figure S13. Whipping. (A)-(C)** The robot first curls up when pulling two cables, and the accumulated elastic potential energy is released to produce a whipping action to pounce a pingpong ball (positioned at variable height).

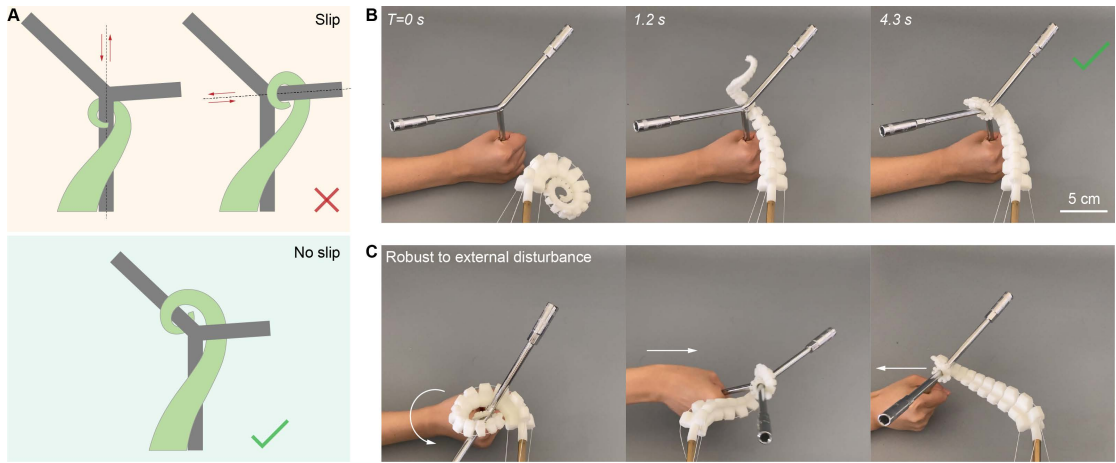


**Figure S14. Non-slipable grasping.** **(A)** Illustration of a non-slipable grasping strategy for the case of a tree-fork-shaped object. **(B)** Image sequence of a 3-cable SpiRob implementing the strategy to grasp a hexagonal wrench. **(C)** Images showing the robustness of the grip under external forces.

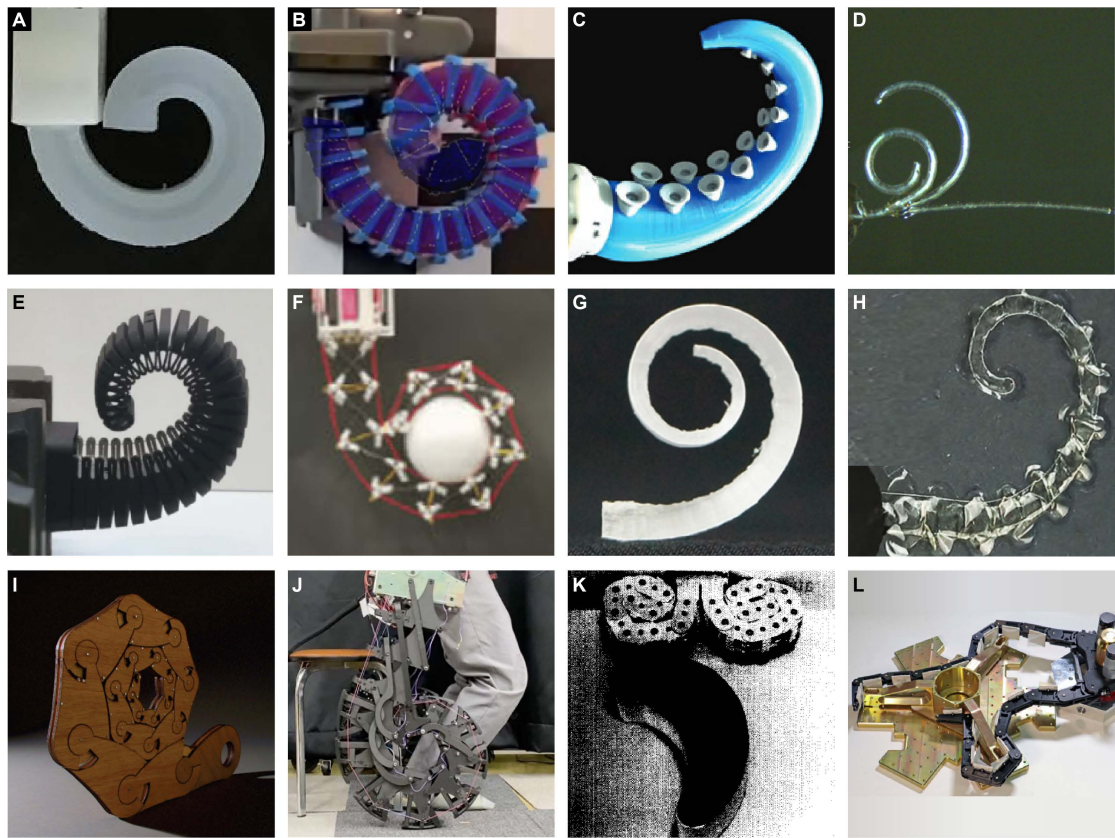


**Figure S15. Spiral-shaped designs in the literature.** (A)-(D) Pneumatically-actuated manipulators: the first two were cast by spiral-shaped molds<sup>[S3,S4]</sup>, while the latter produce a spiral bending when pressurized<sup>[S5,S6]</sup>. (E) and (F) Cable-driven manipulators<sup>[S7,S8]</sup>. (G) thermally-driven tendril-like gripper<sup>[S9]</sup>. (H) Curling HASEL manipulator<sup>[S10]</sup>. (I)-(L) Spiral-shaped designs with rigid links: The first two reproduce the spiral-shaped curling motion<sup>[S11,S12]</sup>, and the last two show the manipulators wrapping objects by uncurling on their surface<sup>[S13,S14]</sup>.

## Supplemental References

- [S1]. Jiang, H., Wang, Z., Jin, Y., Chen, X., Li, P., Gan, Y., Lin, S., and Chen, X. (2021). Hierarchical control of soft manipulators towards unstructured interactions. *Int. J. Robot. Res.* *40*, 411–434. <https://doi.org/10.1177/0278364920979367>.
- [S2]. Coevoet, E., Escande, A., and Duriez, C. (2017). Optimization-Based Inverse Model of Soft Robots With Contact Handling. *IEEE Robot. Autom. Lett.* *2*, 1413–1419. <https://doi.org/10.1109/LRA.2017.2669367>.
- [S3]. Zhang, Z., Wang, X., Meng, D., and Liang, B. (2021). Bioinspired Spiral Soft Pneumatic Actuator and Its Characterization. *J. Bionic Eng.* *18*, 1101–1116. <https://doi.org/10.1007/s42235-021-00075-y>.
- [S4]. Zournatzis, I., Kalaitzakis, S., and Polygerinos, P. (2023). SoftER: A Spiral Soft Robotic Ejector for Sorting Applications. *IEEE Robot. Autom. Lett.* *8*, 7098–7105. <https://doi.org/10.1109/LRA.2023.3315206>.
- [S5]. Xie, Z., Domel, A.G., An, N., Green, C., Gong, Z., Wang, T., Knubben, E.M., Weaver, J.C., Bertoldi, K., and Wen, L. (2020). Octopus Arm-Inspired Tapered Soft Actuators with Suckers for Improved Grasping. *Soft Robot.* *7*, 639–648. <https://doi.org/10.1089/soro.2019.0082>.
- [S6]. Paek, J., Cho, I., and Kim, J. (2015). Microrobotic tentacles with spiral bending capability based on shape-engineered elastomeric microtubes. *Sci. Rep.* *5*, 10768. <https://doi.org/10.1038/srep10768>.
- [S7]. Taylor, I.H., Bawa, M., and Rodriguez, A. (2023). A Tactile-enabled Hybrid Rigid-Soft Continuum Manipulator for Forceful Enveloping Grasps via Scale Invariant Design. In *IEEE International Conference on Robotics and Automation (ICRA)*, pp. 10331–10337. <https://doi.org/10.1109/ICRA48891.2023.10161121>.
- [S8]. Zhang, J., Hu, Y., Li, Y., Ma, K., Wei, Y., Yang, J., Wu, Z., Rajabi, H., Peng, H., and Wu, J. (2022). Versatile Like a Seahorse Tail: A Bio - Inspired Programmable Continuum Robot For Conformal Grasping. *Adv. Intell. Syst.*, 2200263. <https://doi.org/10.1002/aisy.202200263>.
- [S9]. Wang, W., Li, C., Cho, M., and Ahn, S.-H. (2018). Soft Tendril-Inspired Grippers: Shape Morphing of Programmable Polymer–Paper Bilayer Composites. *ACS Appl. Mater. Interfaces* *10*, 10419–10427. <https://doi.org/10.1021/acsami.7b18079>.
- [S10]. Mitchell, S.K., Wang, X., Acome, E., Martin, T., Ly, K., Kellaris, N., Venkata, V.G., and Keplinger, C. (2019). An Easy-to-Implement Toolkit to Create Versatile and High-Performance HASEL Actuators for Untethered Soft Robots. *Adv. Sci.* *6*, 1900178. <https://doi.org/10.1002/advs.201900178>.
- [S11]. Henrich, A. (2021). John Edmark: Art in Motion. *Math. Mag.* *94*, 65–68. <https://doi.org/10.1080/0025570X.2021.1843890>.
- [S12]. Sugiura, S., Unde, J., Zhu, Y., and Hasegawa, Y. (2023). High-strength and flexible mechanism for body weight support. *ROBOMECH J.* *10*, 16. <https://doi.org/10.1186/s40648-023-00255-x>.
- [S13]. Hirose, S., and Umetani, Y. (1978). The development of soft gripper for the versatile robot hand. *Mech. Mach. Theory* *13*, 351–359. [https://doi.org/10.1016/0094-114X\(78\)90059-9](https://doi.org/10.1016/0094-114X(78)90059-9).
- [S14]. Glick, P.E., Van Crey, N., Tolley, M.T., and Ruffatto, D. (2020). Robust capture of unknown objects with a highly under-actuated gripper. In *IEEE International Conference on Robotics and Automation (ICRA)*, pp. 3996–4002. <https://doi.org/10.1109/ICRA40945.2020.9197100>.